Crystal Structures and Their Effects on the Properties of Polyamide 12/Clay and Polyamide 6–Polyamide 66/Clay Nanocomposites

Y. Zhang,[1] J. H. Yang,[1] T. S. Ellis,[2] J. Shi[2]

[1]*Research Institute of Polymer Materials, Shanghai Jiao Tong University, Shanghai 200240, People's Republic of China*
[2]*Delphi Research Labs, Delphi Corporation, 51786 Shelby Parkway, Shelby Township, Michigan 48315*

Received 31 August 2004; accepted 25 June 2005
DOI 10.1002/app.23378
Published online in Wiley InterScience (www.interscience.wiley.com).

ABSTRACT: Both polyamide 12 (PA 12)/clay and polyamide 6–polyamide 66 copolymer (PA 6/6,6)/clay nanocomposites were prepared by melt intercalation. The incorporation of 4–5 wt % modified clay largely increased the strength, modulus, heat distortion temperature (HDT), and permeation resistance to methanol of the polyamides but decreased the notched impact strength. Incorporation of the clay decreased the melt viscosities of both the PA 12 and PA 6/6,6 nanocomposites. Incorporation of the clay increased the crystallinity of PA 6/6,6 but had little effect on that of PA 12, which explained why the clay obviously increased the glass-transition temperature of PA 6/6,6 but hardly had any effect on that of PA 12. The dispersion and orientation of both the clay and the polyamide crystals were studied with transmission electron microscopy, scanning electronic microscopy, and X-ray diffraction. The clay was exfoliated into single layers in the nanocomposites, and the exfoliated clay layers had a preferred orientation parallel to the melt flow direction. Lamellar crystals but not spherulites were initiated on the exfoliated clay surfaces, which were much more compact and orderly than spherulites, and had the same orientation with that of the clay layers. The increase in the mechanical properties, HDT, and permeation resistance was attributed to the orientated exfoliated clay layers and the lamellar crystals. J Appl Polym Sci 100: 4782–4794, 2006

Key words: clay; nanocomposites; orientation; polyamides

INTRODUCTION

In 1980s, Toyota Central R&D Labs disclosed methods for the production of polyamide 6 (PA 6)/clay nanocomposites with *in situ* polymerization.[1–6] First, montmorillonite was intercalated with 12-aminolauric acid or 6-aminolauric acid; then, ε-caprolactam and accelerators were polymerized with the intercalated montmorillonite. By this method, homogeneously dispersed nanocomposites were obtained with exfoliated monolayers about 1 nm thick; this production was proven with X-ray diffraction (XRD) and transmission electron microscopy (TEM). These nanocomposites exhibited superior properties compared to the pure polymers. With a small amount of clay, about 4–5 wt %, the tensile modulus doubled, the tensile strength increased by more than 50%, and the heat distortion temperature (HDT) increased by 80°C.[7] The resistance to water permeation of the PA 6/clay nanocomposites was also superior to that of PA 6.[8] Detailed studies have been carried out on the crystallization of PA/clay nanocomposites,[9–15] the dispersion and orientation of clay,[5,6,16] and the interface between PA 6 and clay.[17]

According to some researchers,[18–25] polymer/clay nanocomposites can be obtained by direct polymer melt intercalation, where polymer chains diffuse into the space between the clay layers. The properties of PA nanocomposites prepared by melt intercalation are comparable to that of *in situ* polymerized PA nanocomposites. PA 6/clay nanocomposites can be prepared by melt intercalation.[25–28] The properties of the nanocomposites are superior to PA 6 in terms of HDT, strength, and modulus. Some work has also been performed to improve the toughness of PA 6/clay nanocomposites. Liu et al.[29] compounded PA 6/clay nanocomposites with maleic anhydride grafted polypropylene to increase the impact strength of the nanocomposites with little sacrifice in strength and modulus. Kojima et al.[7] modified PA 6/clay nanocomposites with diamine to increase the impact strength and elongation at break, with little decrease in strength and modulus. Polyamide 12 (PA 12)/clay nanocomposites have also been prepared by melt intercalation[30,31] and *in situ* polymerization.[32,33] In these nanocomposites, the clay increased the strength and modulus of PA 12 with little sacrifice in impact strength.

Correspondence to: J. Yang (jy13@uakron.edu).
Contract grant sponsor: Delphi Automotive Systems Co.

Another idea was proposed by Kyu et al.[34,35] for obtaining nanocomposites through the incorporation of PA 6/kaolin composites prepared from *in situ* polymerization into commercial PA 6 or polyamide 66 (PA 66). These composites were superior to directly melt-mixed composites in terms of strength, modulus, elongation, and toughness.

The copolymer of polyamide 6 and polyamide 66 (PA 6/6,6) has a lower melting temperature (mp $\approx$ 193°C) than the original polyamides (PAs), which makes it a promising barrier material when one considers that some of the manufacturing technologies for fuel system components rely on thermoforming techniques. Although many PA/clay nanocomposites have been studied, there is no published information about PA 6/6,6/clay nanocomposites. In this study, a PA 6/6,6/clay nanocomposite was prepared by a melt intercalation process. Also, a PA 12/clay nanocomposite was also prepared for parallel studies with the consideration that PA 12 is also used extensively in fuel system components. Although PA 12/clay nanocomposites have been examined in several studies,[30–33] the microstructures of the nanocomposite, especially the crystal structures of the matrix, have not yet been studied in detail. The mechanical and thermal properties and permeability to methanol of the PA 12/clay and PA 6/6,6/clay nanocomposites were studied. The microstructures of the nanocomposites, such as the dispersion and orientation of both the clay layers and the PA crystals, were characterized in detail. The relationship between the structures and properties of the nanocomposites correlated very well.

EXPERIMENTAL

Materials

PA 12 (Grilamid L125) was a commercial product from EMS-CHEMIE (North America), Inc. PA 6/6,6 (Capron CA73ZP) was a low-viscosity and extruder-grade copolymer produced by Honeywell Polymers, Inc. (Morristown, NJ). The clay (Nanomer I.30TC) was a surface-modified montmorillonite mineral from Nanocor, Inc. (Arlington Heights, IL).

Preparation of the samples

The PA resins and the clay were mechanically mixed. Several drops of oil were added into the mixtures of the PA resins and the clay to ensure a uniform mixture. All of the materials were dried in a vacuum oven for at least 12 h at 80°C to avoid moisture-induced degradation reactions. The materials were extruded with a twin-screw extruder at a screw speed of 215 rpm. The temperature profile of the barrel was 220–240–240–240–240–240°C from the hopper to the die. This extrudate was pelletized, dried in a vacuum oven for 12 h at 80°C, and injection-molded into standard samples. The barrel temperature profile in the injection molding was 230–240–240–245°C, and the mold temperature was room temperature.

The practical content of the clay in the nanocomposites were determined as follows. The clay, the neat PA resins, and the nanocomposites were heated in a muffle stove at 800°C until the samples did not lose weight. The weight loss of each of the neat PA resins was 100%, and the weight loss of the clay was 33.9%. The practical contents of the clay in the nanocomposites were obtained by the remaining weights of the nanocomposites divided by 66.1%.

Mechanical properties

Tensile testing for modulus and yield strength was performed with an Instron 4465 tensile tester at a crosshead speed of 5 mm/min (ASTM D 638). Flexural strength and modulus were tested with an Instron 4465 electron tensile tester (Instron Corp., Canton, OH) at a crosshead speed of 2 mm/min (ASTM D 790), and the sample size was $4 \times 10 \times 80$ mm. The notched Izod impact strength was determined with a RAY-RAN impact tester (Ray-Ran Test Equipment Ltd., Nuneaton, UK) (ASTM D 256), and the sample size was $3.2 \times 12.7 \times 63.5$ mm. The depth of the notch was 2.7 mm, and the radius of the notch tip was 0.25 mm. All of the specimens were kept in a sealed desiccator for 24 h at 23°C before the tests. The averages of the test results for five samples were collected.

Thermal properties

The crystallization behavior of the PA resins was studied with a PerkinElmer Pyris 1 DSC (Boston, MA) DSC-7. The sample was heated from 50 to 240°C at 10°C/min, held at 240°C for 5 min, cooled back to 50°C at 10°C/min, and finally heated to 240°C at 10°C/min. HDT was tested according to ASTM D 648. The load on the samples (P) was 1.82 MPa.

DMA

The dynamic mechanical properties of both the neat PA resins and the nanocomposites were tested with a dynamic mechanical thermal analyzer (DMTA IV, Rheometric Scientific, Houston, TX) in a tensile mode at a heating rate of 3°C/min and a frequency of 1 Hz. The elastic moduli [dynamic storage modulus (E') and dynamic loss modulus (E'')] were determined. The glass-transition temperatures (T_g's) were obtained based on the α peaks in the E'' curves.

TEM

The morphologies of the PA nanocomposites were imaged with a transmission electron microscope (Hi-

TABLE I
Mechanical Properties of the PA 12 and PA 6/6,6 Nanocomposites

Sample	Content of clay (wt %)	Yield strength (MPa)	Tensile modulus (MPa)	Flexual strength (MPa)	Flexual modulus (MPa)	HDT at 1.82 MPa (°C)	Notched Izod impact strength (J/m)
PA12	0	43.6	1857	57.0	1315	54.1	149.0
PA 12-C-5	4.20	54.8	2353	80.9	2205	87.0	40.1
PA 6/6,6	0	68.1	2711	99.8	2300	60.0	76.7
PA 6/6,6-C-5	4.56	85.8	3362	125.9	3295	89.2	32.3

PA 12-C-5 is PA 12/Clay nanocomposite with 4.2 wt% of clay. PA 6/6, 6-C-5: PA 6/6, 6/Clay nanocomposite with 4.56 wt% of clay.

tachi H860, Tokyo, Japan). Ultrathin sections, about 100 nm in thickness, were cut from an injection-molded sample 80 mm in diameter and 2 mm in thickness under cryogenic conditions with a microtone.

XRD

XRD intensity curves of the PA resins and the corresponding nanocomposites were obtained at room temperature with a Rigaku Mode D/max-2B diffraction meter (Tokyo, Japan). The X-ray beam was nickel-filtered Cu Kα1 (λ = 0.154 nm) radiation operated at 40kv and 30 mA. Data were obtained from 1 to 40° (2θ) at a scanning rate of 3°/min.

Scanning electron microscopy (SEM)

The notched Izod impact samples were fractured at low temperature, and the fractured surfaces were etched by oxygen plasma at 30 W, 700–720 V, 40 sccm, and 40 mott for 5 min. Then, the etched fractured surfaces were observed with SEM (Hitachi S-2150, Tokyo, Japan).

Permeability measurements

The injection-molded samples (3.2 × 12.7 × 64 mm in size), which were placed in air for 5 months to obtain water absorption equilibrium, were immersed in methanol. Each of the samples was frequently taken out and weighed. The relative weight gains (M_t's) of the samples were calculated with eq. (1):

$$M_t = \frac{W_w - W_d}{W_d} \tag{1}$$

where W_w is the sample weight after an immersion time (t) and W_d is the sample weight before immersion. The diffusion was described with Fick's law. Equation (2) shows the relationship between diffusion coefficient (D) and t at the initial absorption stage:

$$\frac{M_t}{M_m} = \frac{4}{\sqrt{\pi}} \times \sqrt{\frac{Dt}{h^2}} \tag{2}$$

where M_m is the equilibrium relative weight gain of the sample and h is the thickness of the sample.

Rheological properties

The shear viscosities of both the neat PA resins and the corresponding nanocomposites were determined at 220, 240, and 260°C, respectively, with an Instron capillary rheolometer (Instron 4467, Instron Corp., Canton, MA).

RESULTS AND DISCUSSION

Mechanical properties

Table I shows that 4–5 wt % clay obviously increased the strength and modulus of PA 12 and PA 6/6,6. Unfortunately, there was a large decrease in the notched Izod impact strength, especially for PA 12. Figure 1 shows the stress–strain curves of the nanocomposites. PA 6/6,6-C-5 showed brittle fracture without yielding. Both the tensile and impact tests showed an embrittlement effect of the clay.

Thermal properties

HDT

The clay increased the HDT of the PA 12 and PA 6/6,6. By adding 4.2 wt % clay, we increased the HDT of PA 12 by 32.9°C from 54.1 to 87°C. By adding 4.56 wt % clay, we increased the HDT of PA 6/6,6 by 29.2°C from 60 to 89.2°C.

Differential scanning calorimetry

Figure 2(b) shows that the clay increased the crystallization temperature of PA 12 by 14.2°C, and the crystallization peak was also largely narrowed, which indicated a strong heterophase nucleation effect of the

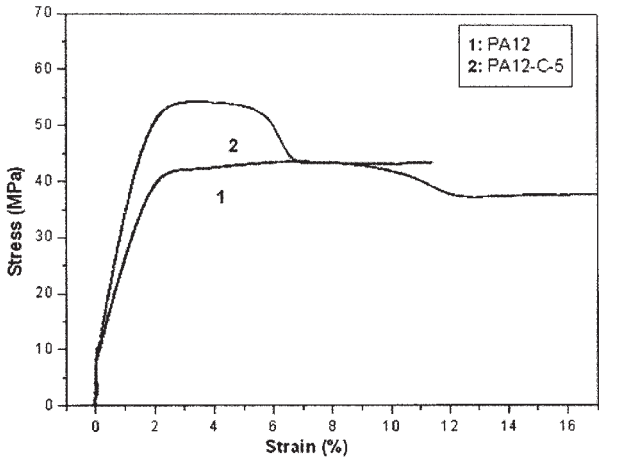

(a)

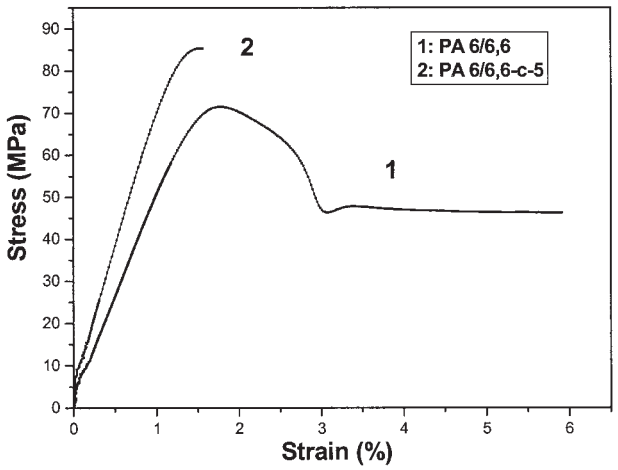

(b)

Figure 1 Stress–strain curves of (a) PA 12 and PA 12-C-5 nanocomposite and (b) PA 6/6,6 and PA 6/6,6-C-5 nanocomposite.

clay. The crystallization enthalpy of PA 12 increased slightly by 3.55% after the incorporation of the clay.

Figure 2(c) shows that both PA 6/6,6 and PA 6/6,6-C-5 had two melting peaks. It was hard to determine the origin of the two peaks based on our studies. Figure 2(d) shows that PA 6/6,6 had two crystallization peaks, which were speculated to have been related to the two melting peaks. However, the PA 6/6,6-C-5 nanocomposite had only one crystallization peak. The crystallization peak was largely narrowed, which showed the strong heterophase nucleation effect of the clay. The crystallization enthalpy of PA 6/6,6 was increased largely by 71.8% after the incorporation of the clay.

Dispersion and orientation of the clay layers

TEM

Round samples 80 mm in diameter and 2 mm in thickness were injection-molded with both the PA 12-C-5 and PA 6/6,6-C-5 nanocomposites. The melts were injected into a mold from the edge of the mold. Ultrathin sections for TEM were cut down at the middle of the samples along both the perpendicular and parallel directions to the sample surfaces under cryogenic conditions.

Figure 3(a) shows the TEM graph of PA 12-C-5 nanocomposite by observation along the direction parallel to the sample surfaces. There are many dark lines in the graph, which are the cross-sections of single or possibly multiple clay platelets. The graph shows that most of the clay particles were exfoliated and the clay layers aligned along the melt flow direction. Figure 3(b) shows the TEM graph of PA 12-C-5 nanocomposite by observation along the direction perpendicular to the sample surfaces. Most of the sections were gray in color without dark lines and clay platelets. This was because of the following reason. Most of the clay layers were parallel to the sample surface, and the ultrathin sections, which were about 100 nm, were much thicker than the clay layers. Thus, nearly all of the electronic beams had to pass through several clay layers, which made nearly all of the graphs show the same gray degree and made it difficult to see the clay platelets. The big particle in Figure 3(c) is one clay particle that was not dispersed well. These observations show that the clay layers in the PA 12 nanocomposite aligned along the melt flow direction and parallel to the sample surfaces.

Figure 3(d–f) shows the TEM graphs of the PA 6/6,6-C-5 nanocomposite. Most of the clay particles were exfoliated. Just as in the PA 12 nanocomposite, the clay layers in the PA 6/6,6 nanocomposite also aligned along the melt flow direction and parallel to the sample surfaces.

XRD

Figure 4 shows the XRD traces of the clay and the nanocomposites. X-rays were used to scan the surfaces of the middle sections of the tensile samples (normal face). The diffraction peak of the clay at $2\theta = 8.32°$ ($d = 1.06$ nm) originated from the (001) crystal planes of the unintercalated clay in the clay sample. The other peak at $2\theta = 3.48°$ ($d = 2.54$ nm) originated from the (001) planes of the intercalated clay. The diffraction curve of the PA 12 showed three peaks at $2\theta = 5.4°$ ($d = 1.63$ nm), 9.4° ($d = 0.94$ nm), and 21.2° ($d = 0.42$ nm), which were related to the (020), (100), and (001) planes, respectively. Here, in the crystal lattice, b axial was along the chain direction. This indicated the γ-form crystal of PA 12.[36–39] The diffraction curve of PA 6/6,6 showed two peaks at $2\theta = 9.8°$ ($d = 0.9$ nm) and 21.1° ($d = 0.42$ nm), which was almost the same with the diffraction curve of the γ-form crystal of both the PA 6[40–45] and PA 66.[46–50] Thus, we can speculate that the two diffraction peaks originated from the

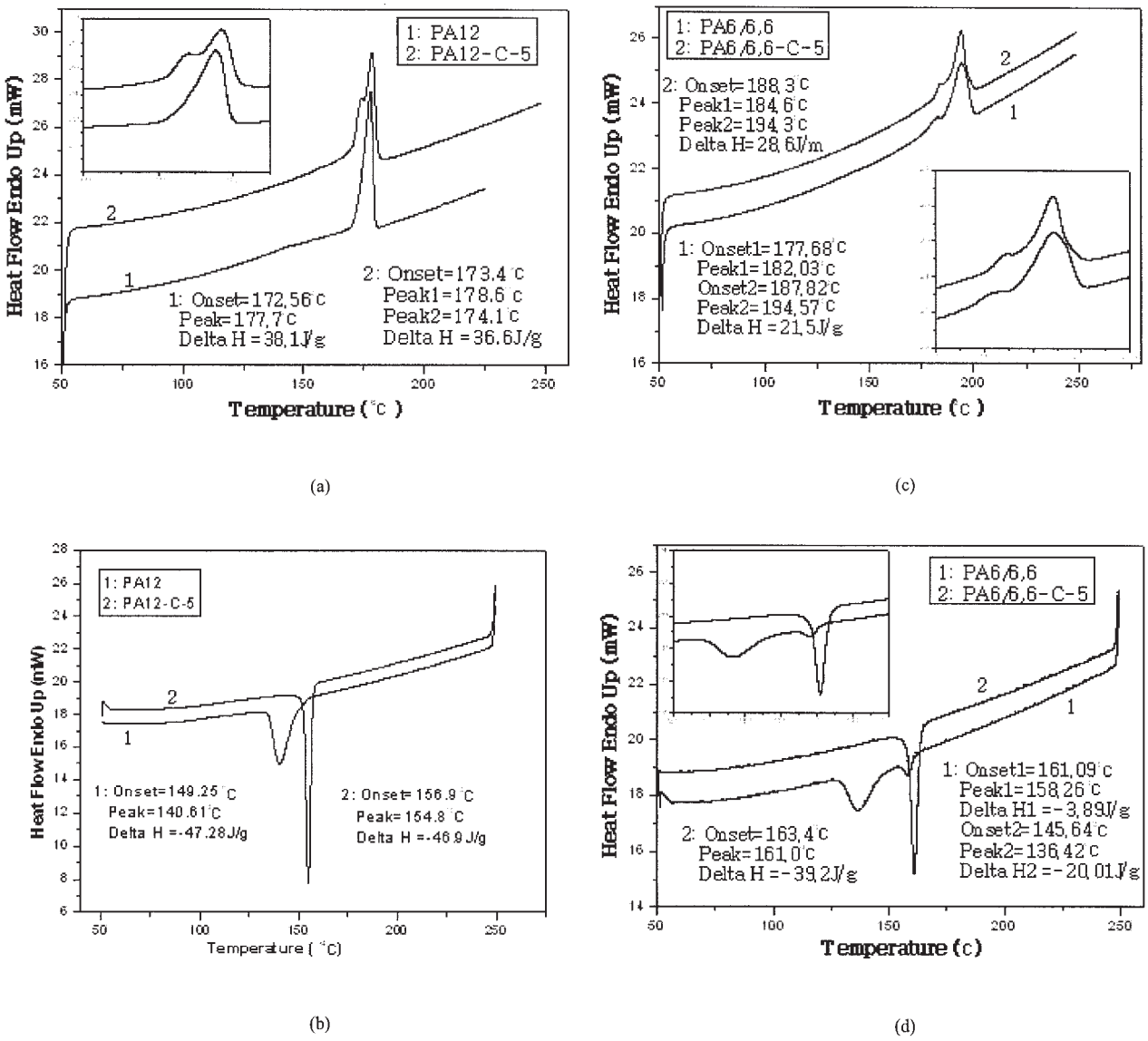

Figure 2 DSC curves of the nanocomposites: (a) melting curves of PA 12 and PA 12-C-5; (b) crystallization curves of PA 12 and PA 12-C-5; (c) melting curves of PA 6/6, 6 and PA 6/6, 6-C-5; (d) crystallization curves of PA 6/6, 6 and PA 6/6, 6-C-5.

(100) and (001) planes of the PA 6/6,6 crystals. Incorporation of the clay did not change the diffraction pattern of the PA crystals, indicating that the clay did not change the crystal form of the PAs.

The diffraction peak at $2\theta = 3.48°$ in the XRD trace of the clay did not appear in those of the PA 12 and PA 6/6,6 nanocomposites. However, there was a high diffraction intensity at small angles of the diffraction curves of both the PA 12 and PA 6/6,6 nanocomposites. The same results were also reported by other researchers.[25,27,31,51,52] The high diffraction intensity at small angles originated from the diffraction between the exfoliated clay layers, which were parallel to the surfaces of the samples. Because there was a large distribution in the distances between the exfoliated clay layers, without preferred distances, there were no diffraction peaks in the area.

Orientation of the crystals

SEM

Figure 5 shows the SEM micrographs of the fractured sample surfaces, which were perpendicular to the flow direction and etched by oxygen plasma. The etching rate of the oxygen plasma to the crystal phases was slower than that to amorphous phases. Thus, in the graphs, the dark regions originated from the etched away amorphous phases, and the white regions are the crystal phases.

Before they were etched, all of the fracture surfaces were very smooth, and the clay could not be seen on

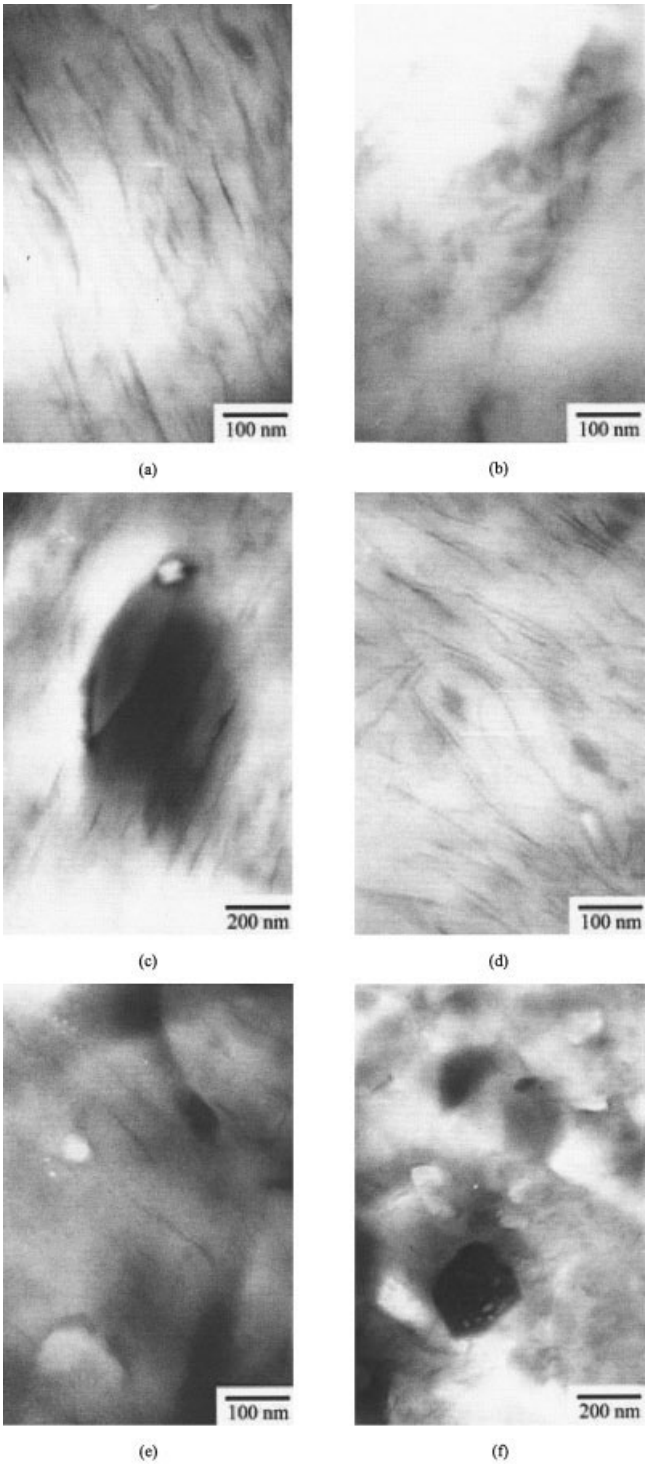

Figure 3 TEM photographs of the nanocomposites: (a) PA 12-C-5, with observation parallel to the surfaces; (b,c) PA 12-C-5, with observation perpendicular to the surfaces; (d) PA 6/6, 6-C-5, with observation parallel to the surfaces; and (e,f) PA 6/6, 6-C-5, with observation perpendicular to the surfaces.

them. Some branched structures were observed on the etched surfaces of both the PA 12 and PA 6/6,6. They were the lamellar PA crystals, which constituted the spherulites of the PAs. The crystals had no orientation. However, on the etched surfaces of the PA 12 and PA 6/6,6 nanocomposites, there were not such branched structures but some obvious lamellar structures that were perpendicular to the fracture surfaces. The lamellar structures should have been composed of both the exfoliated clay layers and PA crystals. The nanocomposite structures seemed to be formed as follows. First, along the melt flow, the exfoliated clay layers were orientated parallel to the sample surface, which was also proven by TEM (shown in Fig. 3). Second, the PA crystals were nucleated on the clay surfaces and grew from the surfaces to the outsides. Because the clay surfaces were full of the growing points of the crystals, the crystals grew homogeneously from all over the clay surfaces to the outsides, forming lamellar crystal structures but not spherulites. Although some publications have shown that clay can obviously de-

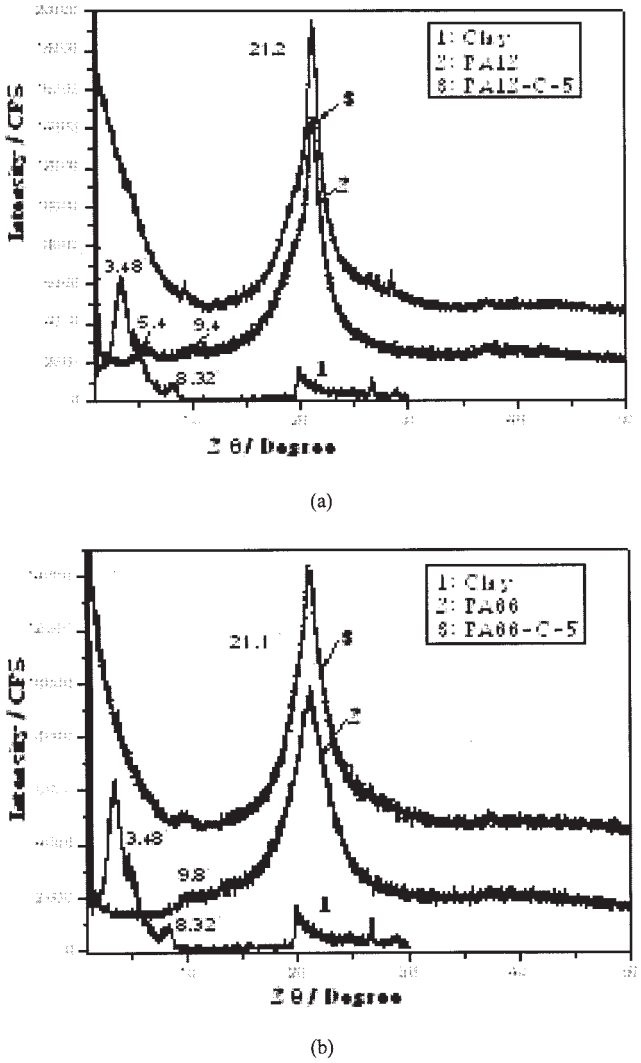

Figure 4 XRD curves of the clay, PAs, and nanocomposites: (a) PA 12-C-5 and PA 12 and (b) PA 6/6, 6-C-5 and PA 6/6, 6.

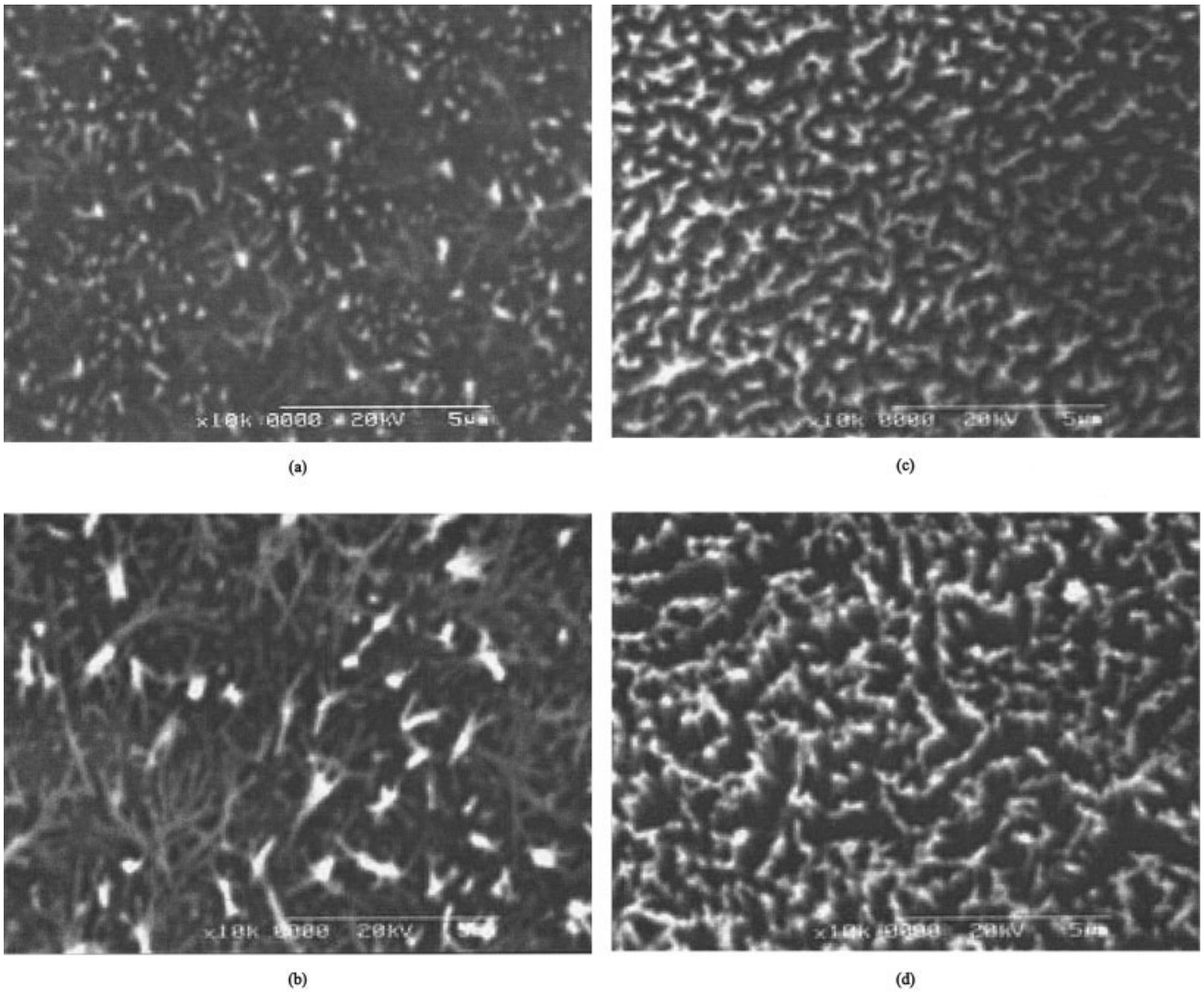

Figure 5 SEM photographs of fracture surfaces etched by plasma: (a) PA 12; (b) PA 6/6, 6; (c) PA 12-C-5; (d) PA 6/6, 6-C-5.

crease the spherulite sizes of polymers,[53,54] no publications have shown the lamellar crystal structures. Yalcin and Cakmak[55] showed that from the surfaces to the cores of injection-molded samples, the crystals of PA 6 changed from lamellar types to spherulites. The incorporation of clay tended to change the spherulites to lamellar crystals.

XRD

Figure 6 shows the XRD curves obtained by the scanning of two perpendicular planes of the samples. The samples were the same as those used for TEM, which were 80 mm in diameter and 2 mm in thickness. One scanned plane was the surface of the injection-molded samples (defined as plane I); the other scanned plane was the fractured surface, perpendicular to the sample surfaces, at the middle of the samples (defined as plane II).

Figure 6(a,c) shows that the XRD traces obtained by the scanning of the two planes of the virgin PAs were almost the same, which indicated that in the virgin PAs, the PA crystals had no preferred orientation. When plane I of both the PA 12 and PA6/6,6 nanocomposites was scanned, there was a high diffraction intensity at small angles. However, when plane II was scanned, there was no such diffraction intensity at small angles [shown in Fig. 6(b,d)]. The high diffraction intensity at low angles originated from the exfoliated clay layers, which was discussed previously. Because the exfoliated clay layers had strong orientation parallel to the sample surfaces, there was no obvious diffraction from the exfoliated clay layers by the scanning of the fractured surfaces, which were parallel to the sample surfaces.

Figure 6(d) shows the diffraction curve of the PA 6/6,6 nanocomposite. When plane I was scanned, there was a big diffraction peak at 20.9°, which was

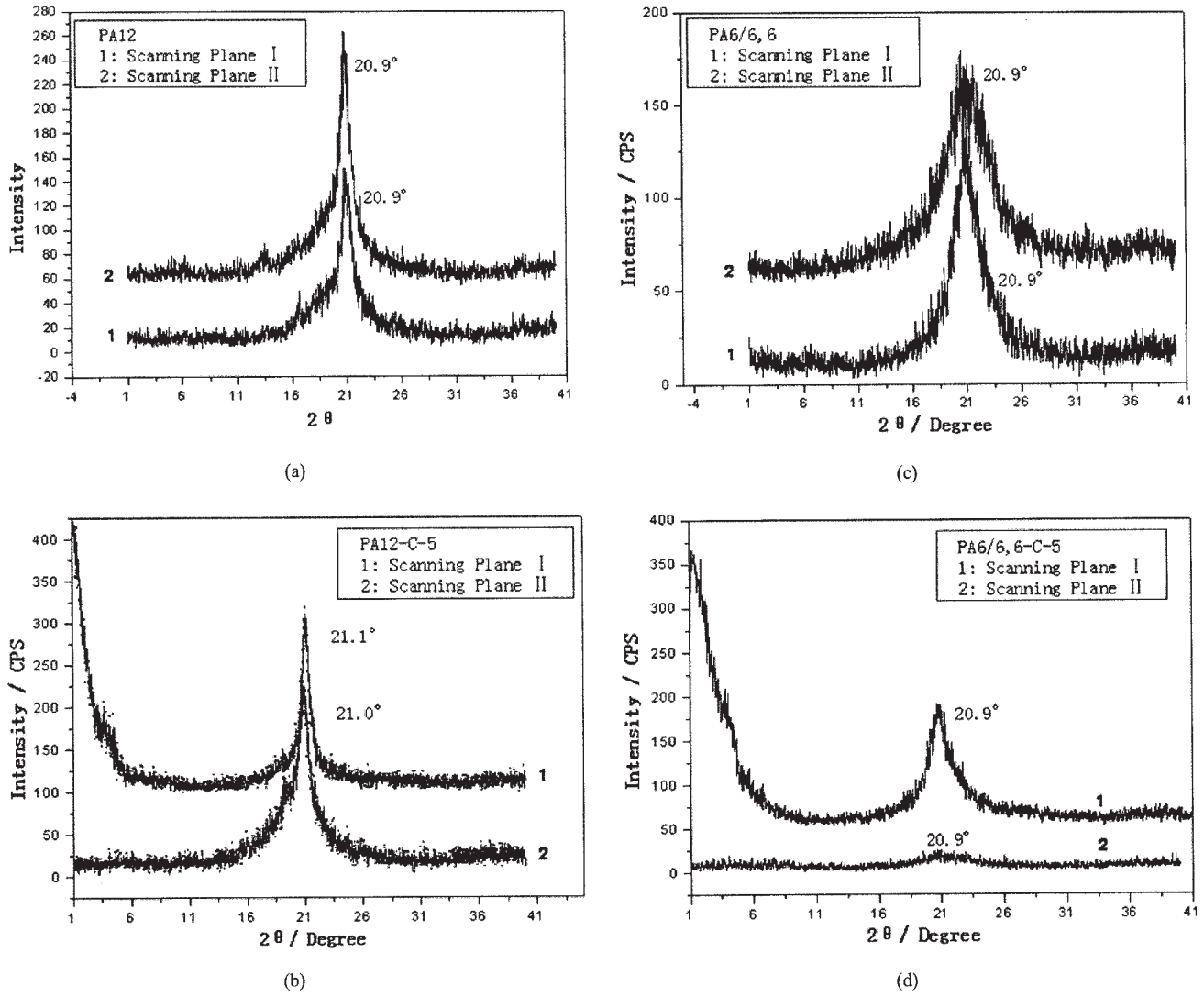

Figure 6 XRD curves obtained by scanning in two directions: (a) PA 12; (b) PA 12-C-5; (c) PA 6/6, 6; (d) PA 6/6, 6-C-5.

attributed to the diffraction between the (001) planes of the PA 6/6,6 crystals. However, when plane II was scanned, the diffraction peak was very low. This indicated that the (001) planes of the PA 6/6,6 crystals in the PA 6/6,6 nanocomposites had a preferred orientation parallel to the surfaces of the samples. Thus, the PA chains also had preferred orientation parallel to the surfaces of the samples. Figure 6(b) indicates that the (001) planes of the PA 12 crystals in the PA 12 nanocomposite had no preferred orientation.

DMA

Figure 7(a) shows E' and E'' versus temperature plots for PA 12 and PA 12 nanocomposite. The α transition peaks in E'' curves response to the T_g. On the basis of Figure 7(a), T_g of the neat PA 12 was 44.3°C, and T_g of the PA 12 nanocomposite was 44.2°C. This indicates that the clay nearly did not change the T_g of PA 12. Figure 7(b) shows that below T_g, the relative E' values of the PA 12 nanocomposite to the neat PA 12 were small (1.2–1.3). Although above T_g, the relative E' values increased greatly, reaching a maximum value of 2.2 around 90°C.

On the basis of Figure 7(c), T_g of the neat PA 6/6,6 was 16.7°C, and T_g of the PA 6/6,6 nanocomposite was 25.9°C. This shows that the clay obviously increased the T_g of PA 6/6,6. Similar to the PA 12 nanocomposite, below T_g, the relative E' values of the PA 6/6,6 nanocomposite to the neat PA 6/6,6 were small (1.0–1.1). However, above T_g, the relative E' values largely increased, reaching a maximal value of 2.2 above 34°C. The same results were also reported earlier for PA 6/clay nanocomposites.[56,57]

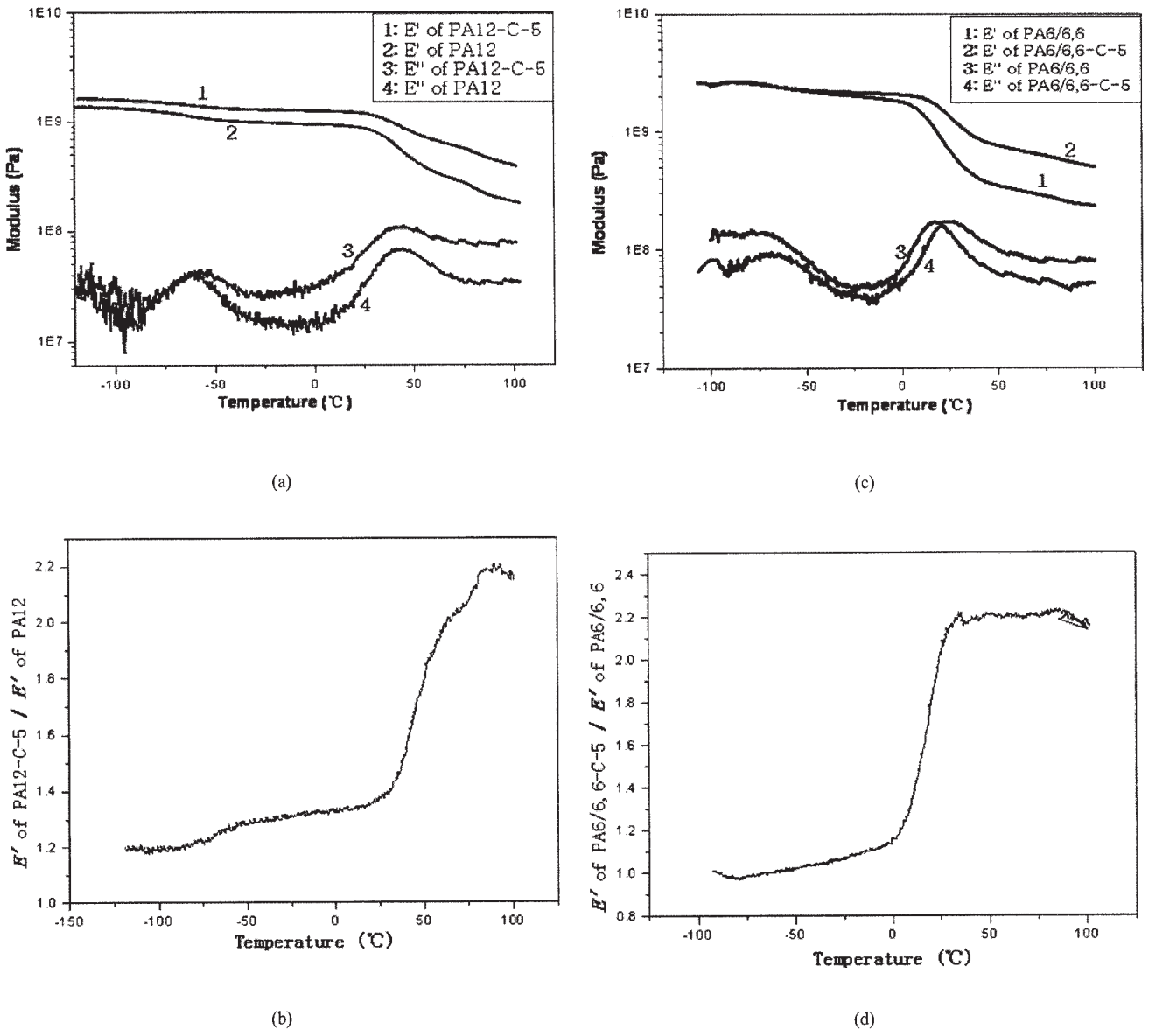

Figure 7 Dynamic mechanical spectra: (a) E' and E'' versus temperature of PA 12 and PA 12-C-5, (b) relative E of PA 12-C-5 to PA 12, (c) E' and E'' versus temperature curves of PA 6/6, and PA 6/6, 6-C-5, and (d) relative E of PA 6/6, 6-C-5 to PA 6/6, 6.

The HDTs of the PAs and PA nanocomposites could be related to their moduli. To make our discussion simple, we imagine them as real elastic materials. In the HDT experiments, the flexural stress (σ), whose value was 1.82 MPa in our experiment, of the samples is shown in eq. (3), and the deflection of the loading nose (δ), whose value was 0.25 mm in ASTM D 648, is shown in eq. (4). Here T is the testing temperature; E is the modulus of the samples, which decreased with increasing temperature; l is the span length (whose value was 100 mm in ASTM D 648); b is the width of the samples (whose value was 3.175 mm in ASTM D 648); and h is the thickness of the sample (whose value was 12.7 mm in ASTM D 648). In the HDT experiment, with increasing temperature, the modulus of the sample decreased. When the modulus of the sample reached one value [we call it the critical modulus (E_0)], the deflection reached the set value and the corresponding temperature was recorded as the HDT of the sample under the exerted load. Dividing eq. (3) by eq. (4), we get eq. (5), which gives us the E_0 value. Substituting the values of all of the parameters in our experiment, we obtain an E_0 value of 955.4 MPa. If we know the relationship between the sample modulus and temperature, we can determine the HDT.

Figure 8 shows the sketch of the relationship between the modulus and temperature. From Figure 8, we can discuss qualitatively the reason why the clay increased the HDT of the PAs. Above T_g, the clay obviously increased the modulus of the PAs. Here, E_0

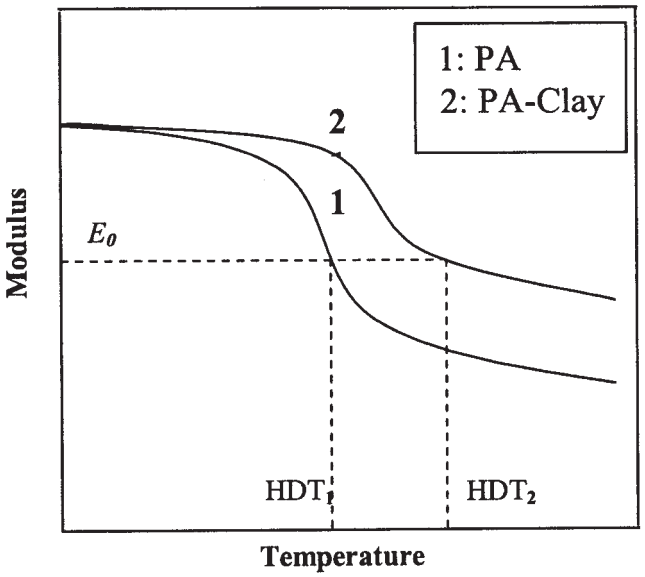

Figure 8 Sketch of the relationship between the modulus and temperature.

= 955.4 MPa for ASTM D 648. Thus, the clay increased the HDT of the PA from HDT_1 to HDT_2. Of course, because the PAs and corresponding nanocomposites showed viscoelastic but not real elastic behavior, there must have been some difference between the experimental value and the predicted value based on this method:

$$\sigma = \frac{3Pl}{2bh^2} \tag{3}$$

$$\delta = \frac{Pl^3}{4E(T)bh^3} \tag{4}$$

$$E(T) = \frac{\sigma l^2}{6h\delta} \tag{5}$$

There have been different reports about the effect of clay on the T_g's of PAs. Some have shown that clay increased the T_g of PA 6,[58] PA 12,[30] and polyamide 1010.[59] They shared the opinion that the strong interaction between clay and PA chains led the clay layers to confine the motion of the polymer chains to increase the T_g's. For example, McNally et al.[30] reported that the modified clay increased the T_g of PA 12 by 20°C; however, the unmodified clay only increased it by several degrees. Some other researches showed that clay decreased the T_g of PA 6[60] and polyamide 1012.[61] Wu et al.'s[61] research showed that clay decreased the crystallinity of polyamide 1012, which they thought led to the decrease of the T_g.

On the basis of our studies, the clay layers are surrounded by the lamellar PA crystals forming along the clay layers. Because the clay is not in the amorphous phases, it has no confining effect on the PA chains in the amorphous phases. Thus, the effect of the clay on the T_g should not be attributed to its confining effect on the PA chains in amorphous phases but to its effect on the crystallinity. The increase in the crystallinity of the semicrystalline polymers can increase the T_g.[62] Not all the polymer chains in amorphous phases are free. Some of them may be attached to crystallites as dangling cilia, tight or loose loops, or tie molecules.[63] Such attachment would restrict the mobility of the chains. In our studies, the clay increased the crystallinity of PA 6/6,6 greatly by 71.8%; thus, it led to an increase in the T_g by 9.2°C. Because the clay had almost no effect on the crystallinity of PA 12, it hardly affected the T_g of PA 12. Although the clay changed the PA 12 crystals from spherulites to lamellar crystals, it seemed that the crystal forms did not affect the T_g.

Permeability

Figure 9 shows the absorption data of the PA 12 and PA 6/6,6 nanocomposites in methanol. Incorporation of the clay increased the permeation resistance of both PA 12 and the PA 6/6,6 to methanol. Both M_m and the absorption speed of the PA 12 and the PA 6/6,6 to methanol decreased with the incorporation of clay.

Figure 10 shows that the incorporation of clay decreased D of PA 12 and PA 6/6,6 in methanol. The diffusion process of small molecules in nanocomposites can be visualized as shown in Figure 11. We reported in the previous paragraphs that the exfoliated clay layers had a preferred orientation parallel to the sample surfaces, and at the same time, the lamellar crystals of PA 12 and PA 6/6,6 growing from the clay surfaces were also parallel to the sample surfaces. Thus, both the clay layers and the crystals in the PA nanocomposites formed a tortuous path for diffusion, which increased the diffusion resistance of both the PA 12 and PA 6/6,6 nanocomposites to methanol.

Rheological properties

Figure 12 shows that both the PA 12 and PA 6/6,6 nanocomposites exhibited shear thinning behavior at 240°C. They showed similar behavior at both 220 and 260°C. Incorporation of the clay obviously decreased the melt viscosities of both the PA 12 and PA 6/6,6 nanocomposites.

Some results that were similar to our results were reported by Cho and Paul.[25] In their study, the incorporation of 5 wt % unmodified montmorillonite had little effect on the melt viscosity of PA 6. However, the incorporation of 5 wt % modified montmorillonite led to a big decrease in the melt viscosity of PA 6. It is not clear what mechanism caused the reduction of melt

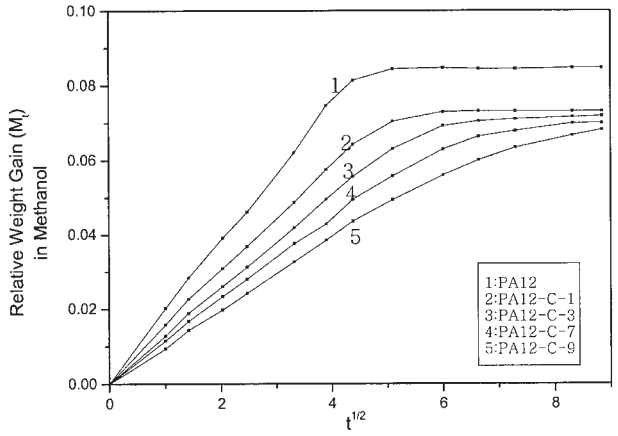

(a)

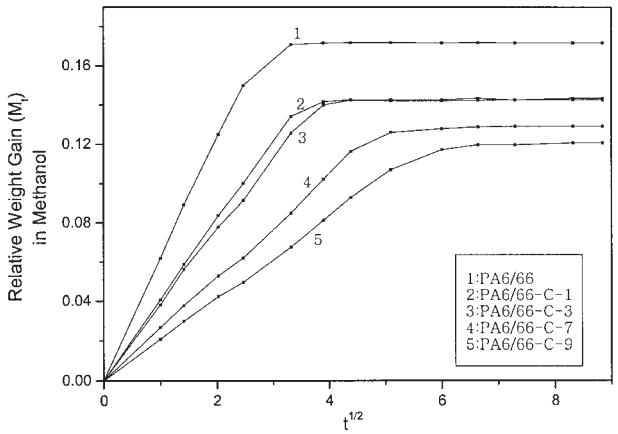

(b)

Figure 9 M_t values of the PA nanocomposites in methanol: (a) PA 12 and (b) PA 6/6,6 nanocomposites.

viscosity. Three factors should be considered. The first factor is the slipping effect between the PAs and the exfoliated clay layers during shear flow. The second factor is that the organic molecules that were used to modify the montmorillonite could partially enter the matrix to reduce the viscosity. The last factor is the possibility of the reduced molecular weight of PA 12 and PA 6/6,6 by degradation, which was stimulated by the degradation of organic molecules.

Structure–property relationships

The incorporation of clay could change the structures of PA 12 and PA 6/6,6 in the following ways. First, the clay could affect the crystallinity of the PAs. For example, the incorporation of 4.56 wt % clay into PA 6/6,6 led to a great increase in the crystallinity by 71.8%. Second, the clay affected the morphology of the crystals. Both the virgin PA 12

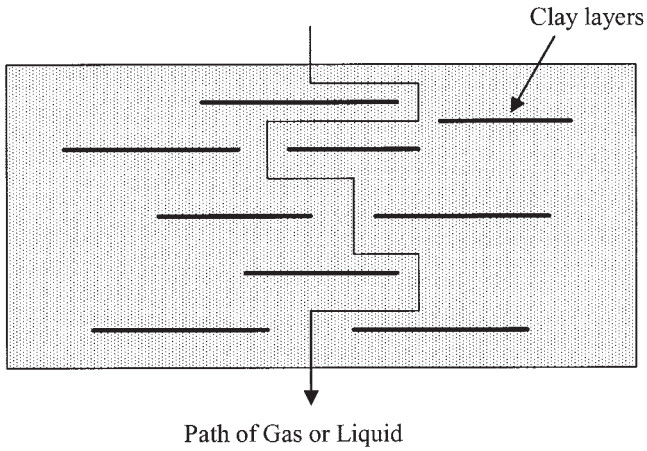

Figure 10 Schematic picture of diffusion in a nanocomposite.

and PA 6/6,6 formed spherulites. However, in the presence of the exfoliated clay layers, the crystals were initiated on the surfaces of the exfoliated clay and grew into lamellar structures surrounding the exfoliated clay layers. In the injection molding, the clay layers had preferred orientation along the melt flow direction. The lamellar crystals had the same orientation as those of the clay.

The lamellar crystals were much more compact and orderly than the spherulites. The exfoliated clay layers together with the lamellar PA crystals contributed to

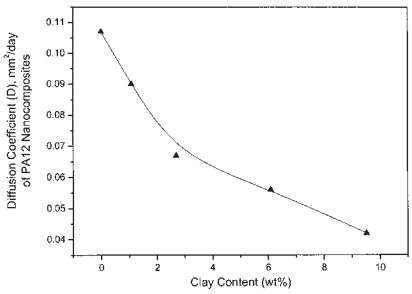

(a)

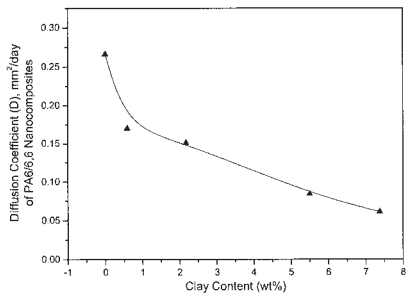

(b)

Figure 11 D of the PA nanocomposites in methanol: (a) PA 12 and (b) PA 6/6,6 nanocomposites.

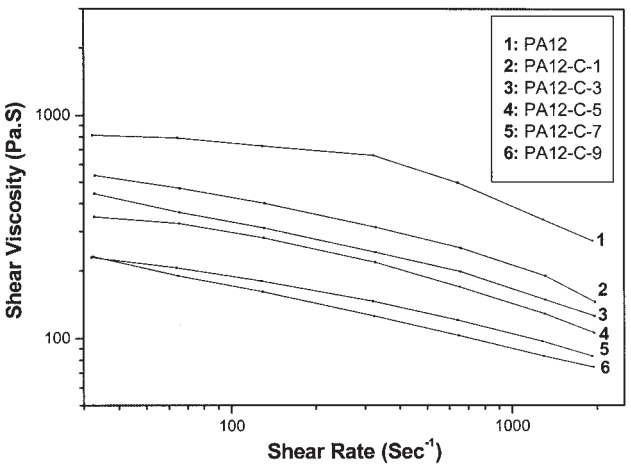

(a)

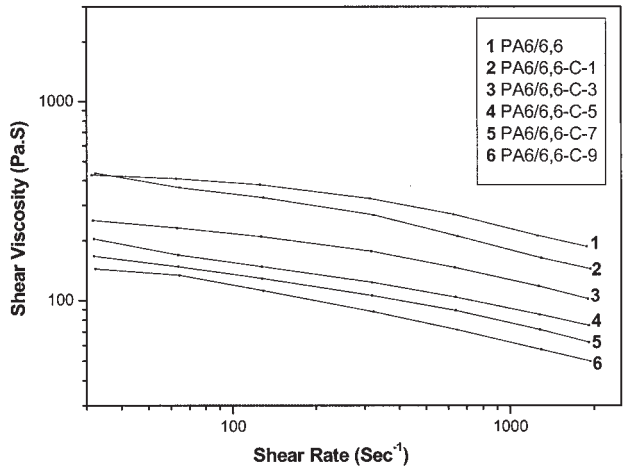

(b)

Figure 12 Melt viscosity as a function of shear rate for the PA 12 and PA6/6,6 nanocomposites at 240°C: (a) PA 12 and (b) PA6/6,6 nanocomposites. The clay contents of PA 12-C-1, 3, 5, 7, 9 nanocomposites are 1.1, 2.69, 4.2, 6.1, 9.5 wt%, respectively. The clay contents of PA 6/6, 6-C-1, 3, 5, 7, 9 nanocomposites are 0.6, 2.2, 4.6, 5.5, 7.4 wt%, respectively.

great increases in strength and modulus. The increased modulus above T_g explained the increased HDT. The oriented clay layers and lamellar crystals parallel to the sample surfaces increased the permeation resistance of the PA nanocomposites to methanol. Also, the increase in the crystallinity contributed to the improvement of all of the properties. Also, although the strength and modulus of the PAs increased, all the structure changes went against the toughness of the PAs.

The polymer/clay nanocomposites gave us a clue to control the structures of the materials. Here, not only did we make lamellar crystals, but we also controlled their orientation by controlling the orientation of the clay layers. The properties of polymer materials relied not only on the polymer chain structures but also on the aggregation structures. Thus, we need polymer chemistry scientists to design and realize the specific chain structures, and we also need polymer physics scientists to design and realize the specific aggregation structures.

CONCLUSIONS

Both PA 12/clay and PA 6/6,6/clay nanocomposites were successfully prepared by melt intercalation. The incorporation of a small amount of clay (4–5 wt %) largely increased the strength, modulus, and HDT values of PA 12 and PA 6/6. However, the notched impact strength was largely decreased (as shown in Table I). The incorporation of clay increased the permeation resistance to methanol of both PA 12 and PA 6/6,6 (shown in Figs. 9 and 10).

The clay had an obvious nucleation effect on the crystallization of both PA 12 and PA 6/6,6. The incorporation of 4.56 wt % clay increased the crystallinity of PA 6/6,6 by 71.8%, but the incorporation of 4.2 wt % clay had little effect on the crystallinity of PA 12 (as shown in Fig. 2).

Most of the clay was exfoliated into single layers in both the PA 12 and PA 6/6,6 nanocomposites (shown in Fig. 3). The exfoliated clay layers had a preferred orientation parallel to the melt flow direction and were parallel to the surfaces of the samples prepared by injection molding (as shown in Figs. 3, 5, and 6). In the nanocomposites, the crystals of PA 12 and PA 6/6,6 were initiated on the surfaces of the exfoliated clay layers and then grew along the clay surfaces, forming lamellar crystals surrounding the exfoliated clay layers. Thus, the spherulites could not be formed in the nanocomposites, although they were formed in the virgin PAs. The lamellar crystals had the same preferred orientation as the exfoliated clay layers (as shown in Fig. 5).

The incorporation of the clay obviously increased the T_g of PA 6/6,6 by 9.2°C; however, it had little effect on the T_g of PA 12. The increase in T_g was attributed to the increase in the crystallinity of PA 6/6,6 but not the confining effect of the clay layers on the polymer chains in amorphous phases because the clay layers were surrounded by the lamellar crystals and were not in the amorphous phases (as shown in Fig. 7).

The authors gratefully acknowledge Delphi Automotive Systems Co. for financial support and materials. They also thank the Instrumental Analysis Center of Shanghai Jiao Tong University for XRD analysis and many helpful discussions.

References

1. Fukushima, Y.; Inagaki, S. Inclusion Phenom 1987, 5, 473.
2. Okada, A.; Fukushima, Y.; Kawasumi, M.; Inagaki, S.; Usuki, A.; Sugiyama, S.; Kurauch, T.; Kamigaito, O. U.S. Pat. 4,739,007 (1988).
3. Kawasumi, M.; Kohzaki, M.; Kojima, Y.; Okada, A.; Kamigaito, O. U.S. Pat. 4,810,734 (1989).
4. Usuki, A.; Kojima, Y.; Kawasumi, M.; Okada, A.; Fukushima, Y.; Kurauch, T.; Kamigaito, O. J Mater Res 1993, 8, 1179.
5. Kojima, Y.; Usuki, A.; Kawasumi, M.; Fukushima, Y.; Okada, A.; Kurauchi, T.; Kamigaito, O. J Polym Sci Part A: Polym Chem 1993, 31, 1755.
6. Kojima, Y.; Usuki, A.; Kawasumi, M.; Okada, A.; Kurauchi, T.; Kamigaito, O. J Polym Sci Part A: Polym Chem 1993, 31, 983.
7. Kojima, Y.; Usuki, A.; Kawasumi, M.; Okada, A.; Fukushima, Y.; Kurauch, T.; Kamigaito, O. J Mater Res 1993, 8, 1185.
8. Kojima, Y.; Usuki, A.; Kawasumi, M.; Okada, A.; Kurauch, T.; Kamigaito, O. J Appl Polym Sci 1993, 49, 1259.
9. Kojima, Y.; Matsuoka, T.; Takahashi, H.; Kurauchi, T. J Appl Polym Sci 1994, 51, 683.
10. Kojima, Y.; Usuki, A.; Kawasumi, M.; Okada, A.; Kurauchi, T.; Kamigaito, O.; Kaji, K. J Polym Sci Part B: Polym Phys 1994, 32, 625.
11. Mathias, L. J.; Davis, R. D.; Jarrett, W. L. Macromolecules 1999, 32, 7958.
12. Fornes, T. D.; Paul, D. R. Polymer 2003, 44, 3945.
13. Liu, X. H.; Wu, Q. J.; Berglund, L. A. Polymer 2002, 43, 4967.
14. Liu, X. H.; Wu, Q. J. Eur Polym J 2002, 38, 1383.
15. Liu, T. X.; Liu, Z. H.; Ma, K. X.; Shen, M. L.; Zeng, K. Y.; He, C. B. Compos Sci Technol 2003, 63, 331.
16. Kojima, Y.; Usuki, A.; Kawasumi, M.; Okada, A.; Kurauchi, T.; Kamigaito, O.; Kaji, K. J Polym Sci Part B: Polym Phys 1995, 33, 1039.
17. Usuki, A.; Koiwai, A.; Kojima, Y.; Kawasumi, M.; Okada, A.; Kurauchi, T.; Kamigaito, O. J Appl Polym Sci 1995, 55, 119.
18. Vaia, R. A.; Ishii, H.; Giannelis, E. P. Chem Mater 1993, 5, 1649.
19. Vaia, R. A.; Jandt, K. D.; Kramer, E. J.; Giannelis, E. P. Macromolecules 1995, 28, 8080.
20. Vaia, R. A.; Giannelis, E. P. Macromolecules 1997, 30, 7990.
21. Vaia, R. A.; Giannelis, E. P. Macromolecules 1997, 30, 8000.
22. Maxfield, M.; Christiani, B. R.; Murthy, S. N.; Tuller, H. U.S. Pat. 5,385,776 (1995).
23. Christiani, B. R.; Maxfield, M. U.S. Pat. 5,747,560 (1998).
24. Kawasumi, M.; Hasegawa, N.; Kato, M.; Usuki, A.; Okada, A. Macromolecules 1997, 30, 6333.
25. Cho, J. W.; Paul, D. R. Polymer 2001, 42, 1083.
26. Dennis, H. R.; Hunter, D. L.; Chang, D.; Kim, S.; White, J. L.; Cho, J. W.; Paul, D. R. Soc Plast Eng Annu Tech Conf Tech Pap 2000, 40, 428.
27. Liu, L.; Qi, Z. N.; Zhu, X. J Appl Polym Sci 1999, 71, 1133.
28. Liu, X. H.; Fan, J. Q.; Qi, Z. N.; 16th Polymer Processing Society Annual Meeting, Shanghai, China, 2000, 604.
29. Liu, X. H.; Wu, Q. J.; Berglund, L. A.; Fan, J. Q.; Qi, Z. N. Polymer 2001, 42, 8253.
30. McNally, T.; Murphy, W. R.; Lew, C. Y.; Turner, R. J.; Brennan, G. P. Polymer 2003, 44, 2761.
31. Reichert, P.; Kressler, J.; Thomann, R.; Mulhaupt, R.; Stoppelmann, G. Acta Polym 1998, 49, 116.
32. Kim, G. M.; Lee, D. H.; Hoffmann, B.; Kressler, J.; Stoppelmann, G. Polymer 2001, 42, 1095.
33. Hoffmann, B.; Kressler, J.; Stoppelmann, G.; Friedrich, C.; Kim, G. M. Colloid Polym Sci 2000, 278, 629.
34. Kyu, T.; Zhou, G. C.; Zhu, Z. L.; Tajuddin, Y.; Qutubuddin, S. J Polym Sci Part B: Polym Phys 1996, 34, 1761.
35. Kyu, T.; Zhou, Z. L.; Zhu, G. C.; Tajuddin, Y.; Qutubuddin, S. J Polym Sci Part B: Polym Phys 1996, 34, 1769.
36. Northolt, M. G.; Tabor, B. J.; Van Aartsen, J. J. J Polym Sci Polym Phys Ed 1972, 10, 191.
37. Cojazzi, G.; Fichera, A.; Garbuglio, C.; Malta, V.; Zannetti, R. Makromol Chem 1973, 168, 289.
38. Inoue, K.; Hoshino, S. J Polym Sci Polym Phys Ed 1973, 11, 1077.
39. Ishikawa, T.; Nagai, S.; Kasai, N. J Polym Sci Polym Phys Ed 1980, 18, 291.
40. Brill, R. Z. Phys Chem B 1943, 53, 61.
41. Holmes, D. R.; Bunn, C. W.; Smith, D. J. J Polym Sci 1955, 17, 159.
42. Kinoshita, Y. Makromol Chem 1959, 33, 1.
43. Vogelsong, D. C. J Polym Sci Part A: Gen Pap 1963, 1, 1055.
44. Arimoto, H.; Ishibashi, M.; Hirai, M.; Chatani, Y. J Polym Sci Part A: Gen Pap 1965, 3, 317.
45. Parker, J. P.; Lindenmeyer, P. L. J Appl Polym Sci 1977, 21, 821.
46. Brill, R. J Prakt Chem 1942, 161, 49.
47. Starkweather, H. W.; Jones, G. A. J Polym Sci Polym Phys Ed 1981, 19, 467.
48. Hirschinger, J.; Miura, H.; Gardner, K. H.; English, A. D. Macromolecules 1990, 23, 2153.
49. Murthy, N. S.; Curran, S. A.; Aharoni, S. M.; Minor, H. Macromolecules 1991, 24, 3215.
50. Ramesh, C. Macromolecules 1999, 32, 3721.
51. Fornes, T. D.; Yoon, P. J.; Hunter, D. L.; Keshkula, H.; Paul, D. R. Polymer 2002, 43, 5915.
52. Yu, Z. Z.; Yang, M. S.; Zhang, Q. X.; Zhao, C. G.; Mai, Y. W. J Polym Sci Part B: Polym Phys 2003, 41, 1234.
53. Liu, Z. J.; Chen, K. Q.; Yan, D. Y. Eur Polym J 2003, 39, 2359.
54. Zhang, Q. X.; Yu, Z. Z.; Yang, M. S.; Ma, J.; Mai, Y. W. J Polym Sci Part B: Polym Phys 2003, 41, 2861.
55. Yalcin, B.; Cakmak, M. Polymer 2004, 45, 2691.
56. Liu, X. H.; Wu, Q. J.; Berglund, L. A.; Lindberg, H.; Fan, J. Q.; Qi, Z. N. J Appl Polym Sci 2003, 88, 953.
57. Uribe-Arocha, P.; Mehler, C.; Puskas, J. E.; Altstadt, V. Polymer 2003, 44, 2441.
58. Yang, F.; Ou, Y. C.; Yu, Z. Z. J Appl Polym Sci 1998, 69, 355.
59. Liu, Z. J.; Zhou, P. L.; Yan, D. Y. J Appl Polym Sci 2004, 91, 1834.
60. Shelley, J. S.; Mather, P. T.; DeVries, K. L. Polymer 2001, 42, 5849.
61. Wu, Z. G.; Zhou, C. X.; Qi, R. R.; Zhang, H. B. J Appl Polym Sci 2002, 83, 2403.
62. Boyer, R. F. J Polym Sci Polym Symp 1975, 50, 189 (especially p 214).
63. Alfrey, T., Jr.; Boyer, R. F. In Molecular Basis of Transitions and Relaxations; Meier, D. J., Ed.; Gordon & Breach: New York, 1978; p 193.